Kim, H.-K. & Santamarina, J. C. (2008). *Géotechnique* **58**, No. 10, 805–814 [**doi:** 10.1680/geot.2008.3724]

Spatial variability: drained and undrained deviatoric load response

H.-K. KIM* and J. C. SANTAMARINA†

Geotechnical properties vary in space. Geostatistical parameters such as the mean, the standard deviation and the correlation length are characteristic for each sediment and formation history. The effects of spatial variability on the drained and undrained shear response of soils are investigated using numerical parametric studies where multiple realisations are tested for selected geostatistical parameters. Results show that the mean undrained shear strength decreases as spatial variability and correlation length increase. Spatial variability prompts strain localisation along neighbouring weak zones under both drained and undrained loading. Heterogeneous contractive media show internal homogenisation during drained deviatoric loading, and the drained shear resistance evolves towards the critical state; media with higher variability and longer correlation length require higher strain to attain internal homogenisation. Anisotropy in spatial correlation causes anisotropy in shear strength. An intermediate drainage condition emerges in spatially varying media whereby local drainage may develop during globally undrained shear; local drainage affects the load–deformation response.

KEYWORDS: failure; numerical modelling & analysis; pore pressures; shear strength; statistical analysis

Les propriétés géotechniques varient dans l'espace. Les paramètres de géostatistique, comme par exemple la moyenne, l'écart type et la longueur de corrélation sont des caractéristiques propres à l'histoire de chaque sédiment et de chaque formation. On examine les effets de la variabilité spatiale sur la réponse au cisaillement du sol drainé et non drainé, sur la base d'études de paramètres numériques dans lesquels on teste de multiples réalisations sur le plan de paramètres de géostatistique sélectionnés. Les résultats indiquent que la résistance moyenne au cisaillement du sol non drainé diminue au fur et à mesure de l'augmentation de la variabilité spatiale et de la longueur de corrélation. La variabilité spatiale engendre la localisation des contraintes le long de zones de faiblesse avoisinantes, en présence de charges drainées et non drainées. Les milieux à contraction hétérogène indiquent qu'une homogénéisation interne en présence de chargements déviatoriques et de la résistance au cisaillement des sols drainés évolue vers l'état critique ; les milieux présentant une variabilité majeure et une longueur de corrélation supérieure nécessitent une sollicitation supérieure pour obtenir une homogénéisation interne. L'anisotropie dans la corrélation spatiale engendre une anisotropie de la longueur de cisaillement. Un drainage intermédiaire se déclare dans des milieux qui varient sur le plan spatial, dans le cadre duquel un drainage local pourra se produire au cours d'un cisaillement dans une sol globalement non drainé ; le drainage local affecte la réponse charge–déformation.

INTRODUCTION

The spatial variability of soil properties is determined by the soil formation history, and it is readily observed in in situ test data (Tang, 1979; Harr, 1987; Kulhawy, 1992; Ravi, 1992; DeGroot & Baecher, 1993; Hegazy *et al.*, 1996; Lacasse & Nadim, 1996; Phoon & Kulhawy, 1999), petrographic image analysis (Antonellini *et al.*, 1994a), digital image correlation analyses of triaxial tests (Rechenmacher *et al.*, 2005; Rechenmacher & Medina-Cetina, 2007), cross-sectional images of impregnated soils (Jang *et al.*, 1999), X-ray tomography (Antonellini *et al.*, 1994b) and electrical needle probe profiles (Cho *et al.*, 2004). The consequences of spatial variability for the quasi-static resistance (Yoshida *et al.*, 1993; Vaid *et al.*, 1995; Hoeg *et al.*, 2000; Vaid & Sivathayalan, 2000) and the dynamic resistance are extensively documented (Ladd, 1974; Mulilis *et al.*, 1975; Townsend, 1978; Ishihara, 1993; Popescu *et al.*, 1997, 2005).

Spatial variability can be captured in statistical parameters such as the coefficient of variation (COV) and the correlation length (Vanmarcke, 1977; Phoon & Kulhawy, 1999). The COV is defined as the ratio between the standard deviation and the mean value. The correlation length is the distance where the spatial autocorrelation decays by $1/e$, and it indicates the spatial scale of material heterogeneity. Published ranges for the COV and the correlation length for various soil properties can be found in Harr (1987), DeGroot (1996), Lacasse & Nadim (1996), Phoon & Kulhawy (1999), and Jones *et al.* (2002).

Conventional probabilistic approaches assume a representative equivalent volume of size much greater than the correlation length to obtain estimates of the effective shear strength (Ang & Tang, 1975; Harr, 1987). Effective mixture models for non-linear materials are summarised in Zaoui (2002). However, these approaches fail to anticipate emergent phenomena such as the localised deformation observed in heterogeneous materials under deviatoric loading (Nübel & Karcher, 1998; Griffiths *et al.*, 2002; Hicks & Samy, 2002; Cho *et al.*, 2004; Andrade & Borja, 2006).

The goal of this study is to gain new understanding of the effects of spatial variability on the load–deformation response of contractive and dilative soils subjected to drained and undrained loading. The focus is not on the effect that the selected distribution has on the ensuing material properties or on the tail of the distribution, which would be important for risk analyses. Instead, emphasis is placed on identifying potential emergent phenomena that may control the global response. The complete study is documented in Kim (2005).

Manuscript received 17 May 2006; revised manuscript accepted 17 July 2008.
Discussion on this paper closes on 1 June 2009, for further details see p. ii.
* Department of Civil and Environmental Engineering, Kookmin University, Seoul, South Korea.
† School of Civil and Environmental Engineering, Georgia Institute of Technology, Atlanta, USA.

NUMERICAL METHOD AND MATERIAL MODEL

The research is implemented using the finite element program ABAQUS (HKS, 2006). The simulated test in all cases is a strain-controlled plane-strain biaxial compression condition. The square mesh consists of 100 × 100 four-node plane-strain elements to minimise geometric effects caused by correlated random variability.

A simple constitutive model is sought for this study, which can capture the stress-dependent soil strength, pre-failure plastic strain, and pore water pressure development. Therefore the Modified Cam-Clay material model is selected herein (Roscoe & Burland, 1968). The five model parameters are: the consolidation parameters (slope of the normal consolidation line λ, slope of the swelling-recompression line, κ, and specific volume V_1); the drained strength parameter (stress ratio at critical state M); and the initial elastic parameter (Poisson's ratio ν or elastic shear modulus G). Constitutive model parameters and boundary conditions are summarised in Table 1; the selected values correspond to a silty clay.

Random variability is imposed on the initial void ratio e_0 at $\sigma'_0 = 100$ kPa; variability in e_0 corresponds to variance in strength. Experimental results suggest that the void ratio probability density function approaches the log-normal distribution (Jang, 1997; Yang, 2005), or exponential-type distribution skewed towards the looser elements (Shahinpoor, 1981; Bhatia & Soliman, 1990; Nübel & Karcher, 1998). To avoid extreme values in e_0, a bounded uniform distribution is selected that satisfies preselected values of the mean and the standard deviation, and generate multiple realisations of the two-dimensional correlated scalar random e_0 fields using the matrix decomposition technique. The procedure is outlined below (for details see Fenton, 1994; El-Kadi & Williams, 2000; Vio *et al.*, 2001):

(*a*) Generate the covariance matrix **A** for the given standard deviation σ, correlation length L for an exponential autocorrelation function, and the distance d_{ij} between points i and j:

$$A_{ij} = \sigma^2 \mathrm{e}^{-\frac{1}{L}|d_{ij}|} \tag{1}$$

(*b*) Apply the Choleski decomposition to obtain the matrix **C**:

$$\mathbf{A} = \mathbf{C}C^{\mathrm{T}} \tag{2}$$

Table 1. Numerical study: model, material parameters and parametric study

Boundary conditions (all cases)

Strain-controlled vertical z-compression Constant confinement: $\sigma_0 = 100$ kPa Plane strain in y-direction: $\varepsilon_y = 0$ No friction against boundaries: $\tau_{xz} = 0$ at boundaries Element type: four-node, pore-pressure-coupled, plane-strain element Mesh: 100 × 100 elements	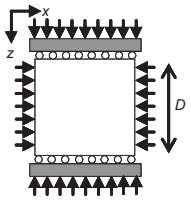

Modified Cam-Clay model parameters

Slope of the normal consolidation line, λ	0·174
Slope of the swelling-recompression line, κ	0·026
Specific volume, V_1	2·824 ($e_1 = 1{\cdot}824$)
Stress ratio at critical state, M	1·0 ($\phi' = 25°$)
Poisson's ratio at 1 kPa, $\nu_{1\mathrm{kPa}}$	0·3
Preconsolidation pressure parameter, a_0	$a_0 = \frac{1}{2}\exp\left(\frac{e_1 - e_0 - \kappa \ln P_{\mathrm{init}}}{\lambda - \kappa}\right)$ where P_{init} is initial confining pressure.

Random variable (all cases): initial void ratio e_0

Cases reported in this paper:

Drainage condition	*Topic*	*e_0 distribution and range*		*Relative correlation length, L/D*	*Figure*
Undrained	Binary mixtures	Binary	0·90 and 1·00	∼0	1, 2
Undrained	Contractive and dilative media	Uniform	0·80–1·00	0·1	3
Undrained	Dilative medium	Uniform	0·70–0·80	0·1	4
Undrained	Strain localisation	Uniform	0·80–1·00	∼0, 0·1	5
	Local drainage	Uniform	0·65–0·75	0·1	
			0·80–1·00		6
Undrained	Anisotropic heterogeneity	Uniform	0·80–1·00	$L_{\mathrm{H}}/L_{\mathrm{V}} = 0{\cdot}1, 0{\cdot}2, 0{\cdot}5, 1{\cdot}0, 2{\cdot}0, 5{\cdot}0, 10{\cdot}0$	7
Undrained	Variability	Uniform	0·87–0·93	0·16	8
			0·85–0·95		
			0·83–0·97		
			0·80–0·10		
Undrained	Correlation length	Uniform	0·80–1·00	∼0, 0·02, 0·04, 0·10, 0·16	9
Drained	Contractive medium	Uniform	0·80–1·00	0·1	10, 11, 12
Drained	Variability and correlation length	Uniform	0·80–0·90	∼0, 0·1	13
			0·85–0·95		
			0·90–1·00		
Drained	Dilative medium	Uniform	0·70–0·80	0·1	14, 15, 16

(*c*) Calculate the Gaussian scalar random field $X(\cdot)$:

$$X(\boldsymbol{l}) = C\varepsilon(\boldsymbol{l}) + T(\boldsymbol{l}) \tag{3}$$

where $\boldsymbol{l}$ is the location vector, $T(\cdot)$ is the trend and $\varepsilon(\cdot)$ is the uncorrelated Gaussian random field of zero mean and unit variance.

(*d*) Finally, transform the generated Gaussian random field to the uniform distribution random field (Grigoriu 1984; Yamazaki & Shinozuka, 1988):

$$R(\boldsymbol{l}) = F_R^{-1}\{F_X[X(\boldsymbol{l})]\} \tag{4}$$

where $F_X(\cdot)$ is the Gaussian probability distribution function, and $F_R(\cdot)$ denotes a marginal probability distribution function for the non-Gaussian scalar random field $R(\cdot)$.

There are two length scales in these realisations, the specimen size D and the internal scale of heterogeneity L: both scales are combined into the relative correlation length L/D.

Once a realisation is generated at $\sigma_0' = 100$ kPa confining stress, the deviatoric load is imposed in strain-controlled mode. The free horizontal displacement for top and bottom nodes simulates frictionless boundary conditions. Drainage conditions depend on the rate of pore pressure generation associated with the imposed strain rate, and the rate of pore pressure diffusion, which is related to (drainage length)^2/(consolidation coefficient). As there are two length scales D and L, three different drainage conditions are modelled:

(*a*) locally and globally undrained (called 'undrained' herein)
(*b*) locally drained yet globally undrained
(*c*) locally and globally drained (called 'drained' herein).

The data gathered for all realisations are analysed using ensemble statistics to determine the effects of spatial variability on soil strength. Table 1 summarises the parameters and conditions assumed in all the simulations shown in this paper.

UNDRAINED RESPONSE

This section describes the results of numerical simulations conducted to investigate the undrained stress–strain response of spatially varying media subjected to deviatoric loading.

Uncorrelated binary mixture

The case of random binary mixtures made of strong and weak materials is studied first. The initial void ratios at 100 kPa confinement are $e_0 = 0{\cdot}9$ for the strong elements (corresponding undrained strength $q_{\text{peak}} = 114$ kPa) and $e_0 = 1{\cdot}0$ for the weak elements ($q_{\text{peak}} = 63$ kPa). The volume fraction of the weak material is varied from $V_{\text{weak}} = 0\%$ (homogeneous specimen made of strong material only) to $V_{\text{weak}} = 100\%$ (homogeneous specimen made of weak material only). Each mixture is randomly generated as follows: a random number R from 0 to 1 is associated to each cell; cells with $R \leqslant V_{\text{weak}}$ are assigned $e_0 = 1{\cdot}0$; the remaining cells are assigned $e_0 = 0{\cdot}9$. The study involves 20 realisations of each mixture.

Figure 1 shows the resulting stress–strain curves for $V_{\text{weak}} = 10\%$ and 50%. Results are presented in terms of the mean invariant quantities at the boundaries,

$$p' = \frac{1}{3}\left(\bar{\sigma}_x' + \bar{\sigma}_y' + \bar{\sigma}_z'\right)$$

$$q = \frac{1}{\sqrt{2}}\left[\left(\bar{\sigma}_x' - \bar{\sigma}_y'\right)^2 + \left(\bar{\sigma}_x' - \bar{\sigma}_z'\right)^2 + \left(\bar{\sigma}_y' - \bar{\sigma}_z'\right)^2\right]^{1/2} \tag{5}$$

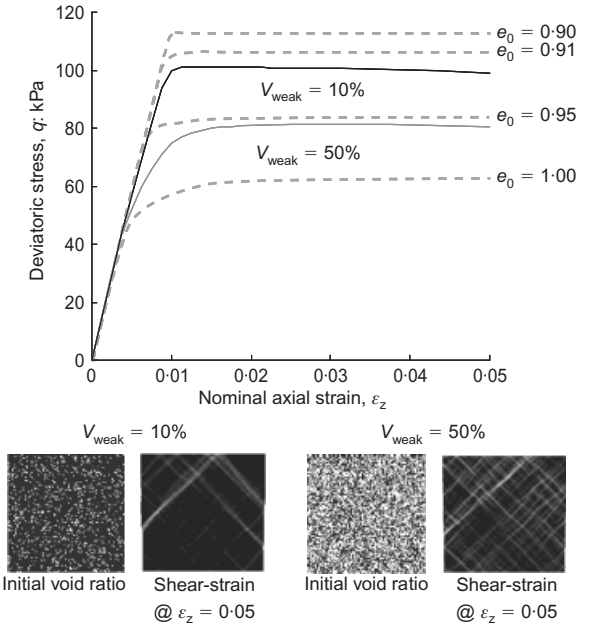

Fig. 1. Undrained shear strength for binary mixtures with very short correlation length: stress–strain curves shown for two volume fractions of the weak material. Dotted lines correspond to homogeneous media with different void ratios. Shear strength of the strong component ($e_0 = 0{\cdot}9$) is $q_f = 114$ kPa; that of weak component ($e_0 = 1{\cdot}0$) is $q_f = 63$ kPa

where $\bar{\sigma}_x'$, $\bar{\sigma}_y'$ and $\bar{\sigma}_z'$ are the mean principal effective stresses applied normal to boundaries. The response for four homogeneous cases at $e_0 = 0{\cdot}90$, $0{\cdot}91$, $0{\cdot}95$ and $1{\cdot}00$ are superimposed on the figure for comparison. Note that homogeneous media with initial void ratios $e_0 = 0{\cdot}91$ and $0{\cdot}95$ exhibit higher shear strength than the $V_{\text{weak}} = 10\%$ and 50% heterogeneous media with the same arithmetic mean void ratios $\mu[e_0] = 0{\cdot}91$ and $0{\cdot}95$. Shear strain distributions and the associated stress–strain curves in Fig. 1 show the development of strain localisation and some post-peak softening behaviour in mixtures with $V_{\text{weak}} = 10\%$ (see also Andrade & Borja, 2006).

Figure 2 shows the one-sigma ranges for the peak shear strength values. Several mixture model predictions are shown as well. It can be observed that the mean undrained shear strength of random mixtures is lower than (a) the arithmetic mean of the shear strength $\mu[q_{\text{peak}}]$ and (b) the

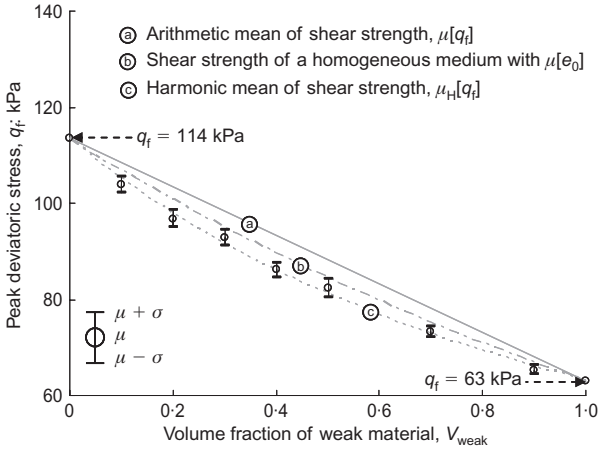

Fig. 2. Peak undrained shear strength for binary mixtures with very short correlation length. Shear strength of strong component is $q_f = 114$ kPa; that of weak component is $q_f = 63$ kPa

shear strength of homogeneous media with the same arithmetic mean void ratio $\mu[e_0]$. Indeed, the mean strength is well predicted by the harmonic mean $\mu_H[q_{peak}]$ of the local undrained strength values (line 'c'). This observation suggests the propagation of failure along neighbouring 'weak zones' in the specimen.

Correlated random fields: localisation of shear strain

A sequence of simulations is conducted using two-dimensional correlated scalar random fields of initial void ratio e_0 (uniform distribution). The load–deformation response and associated shear strain fields reveal the following sequence of events when these plane-strain realisations are subjected to undrained deviatoric loading (see Fig. 3 for a contractive specimen and Fig. 4 for a dilative specimen).

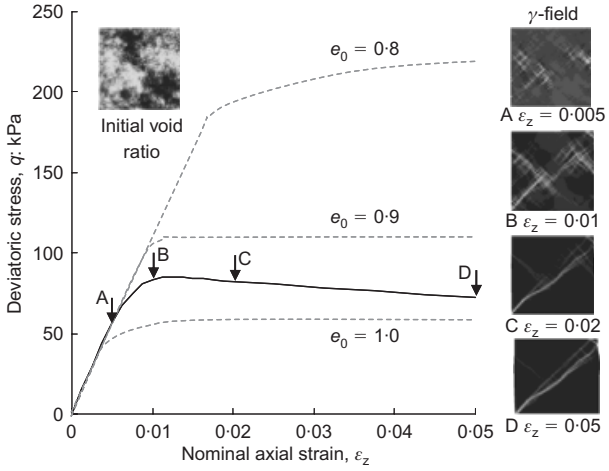

Fig. 3. Internal strain evolution in heterogeneous medium subjected to undrained deviatoric loading. Initial void ratio range $e_0 = 0{\cdot}8–1{\cdot}0$, $L/D = 0{\cdot}1$. Note: $e_{cs} = 0{\cdot}92$ for $\sigma'_0 = 100$ kPa. Therefore this specimen contains both contractive and dilative elements. Lighter colour indicates higher shear strain or void ratio. Dotted lines are for homogeneous media at the indicated void ratios

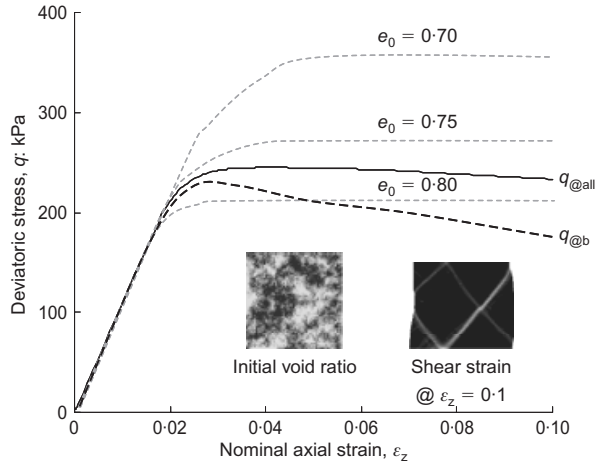

Fig. 4. Stress–strain response of dilative heterogeneous medium subjected to undrained deviatoric loading. Initial void ratio range $e_0 = 0{\cdot}7–0{\cdot}8$, $L/D = 0{\cdot}1$. Note: $e_{cs} = 0{\cdot}92$ for $\sigma'_0 = 100$ kPa. Therefore all elements in this specimen are on the dilative side of critical state. Lighter areas indicate higher shear strain or void ratio. Solid line shows q calculated from mean vertical and horizontal effective stresses of whole medium; thick black dotted line shows q calculated from mean effective normal stresses on boundaries. Dotted grey lines are for homogeneous media with different void ratios

(*a*) Multiple shear strain localisations are apparent before the peak stress.
(*b*) More focused shear strain localisations develop along weak elements near the peak stress.
(*c*) Shear localises in a few bands after the peak.

(Related experimental plane-strain data can be found in Vardoulakis *et al.*, 1978; Han & Vardoulakis, 1991; Finno *et al.*, 1997; Alshibli *et al.*, 2003; Rechenmacher, 2006). These observations may vary for other boundary conditions (e.g. Desrues *et al.*, 1996; Desrues, 1998; Lade & Wang 2001).

The interpretation of measured quantities becomes more difficult in spatially varying media. Fig. 4 shows the load–deformation response where q is computed in terms of boundary values ($q_{@b}$) and as an average for the whole specimen ($q_{@all}$). Whereas $q_{@all}$ appears to be the expected response, $q_{@b}$ is the response measured in laboratory experiments (see complementary experimental and numerical results in Rechenmacher & Medina-Cetina 2007).

Figure 5 presents the void ratio distribution inside the localised shear zones in the strongest and the weakest realisations, out of 40 realisations tested for two different correlation lengths ($L/D = 0{\cdot}1$ and ~ 0) and the same initial void ratio distribution ($e_0 = 0{\cdot}8$ to $1{\cdot}0$, uniform distribution). The overwhelming presence of weak elements in shear zones seen in Fig. 5 confirms the role of weak elements in strain localisation. The cumulative void ratio distribution for elements in shear zones is closer to the whole medium void ratio distribution for realisations that exhibit higher global strength. It is important to emphasise that localisation phenomena identified in this study are the direct consequence of spatial variability rather than strain-softening local response.

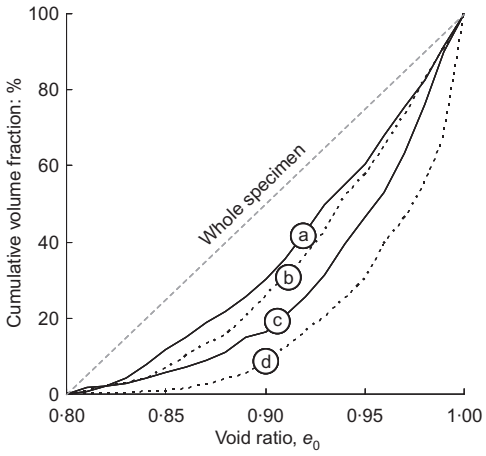

	a	b	c	d
L/D	0·005	0·005	0·100	0·100
q_f: kPa	111·1 (strongest)	105·2 (weakest)	103·3 (strongest)	69·2 (weakest)
Void ratio field (e_0 = 0·8 to 1·0)				
γ field @ ε_z = 0·1				

Fig. 5. Cumulative void ratio distribution for elements presumed in local shear zones during undrained deviatoric loading. Elements in presumed shear localisation zones are selected by sorting all elements according to shear strain and extracting top 5% of all elements that experienced the highest shear strain. Lighter colour indicates higher shear strain or void ratio

The initial void ratio fields and the corresponding shear strain fields in each case are shown as well. The zones where shear strains localise cannot be anticipated from a cursory observation of the initial void ratio field when the correlation length is short. Narrower shear strain zones develop in media with short correlation length L/D.

Local drainage effects

The pore pressure generated in spatially varying media subjected to undrained loading is not necessarily homogeneous (Popescu *et al*., 1997, 2005). Can local drainage in a globally undrained specimen affect the stress–strain response? Fig. 6 shows four stress–strain curves for correlated random media subjected to globally undrained deviatoric loading, with and without local drainage. The 'locally drained yet globally undrained' condition is imposed by shearing very slowly while keeping no-drainage global boundaries; the excess pore pressure development throughout the specimen is homogeneous. Results in Fig. 6 and similar ones obtained as part of this study suggest that local drainage allows strength gain in weak zones whereas dilation and strength loss takes place in stronger zones. The global consequences of this trade-off include minor changes in strain localisation and shear strength.

Anisotropy in spatial correlation

Anisotropy in spatial correlation may favour failure (e.g. Hicks & Onisiphorou, 2005). Numerical simulations are conducted by varying the ratio of the horizontal to the vertical correlation length in random fields. In all cases, the specimen initial void ratio follows a uniform distribution in the $e_0 = 0{\cdot}8$ to $1{\cdot}0$ range, and the longest of the two correlation lengths is kept constant at $L/D = 0{\cdot}1$ to prevent numerical bias. Twenty realisations are tested for each condition. The mean trend and one-sigma ranges of the undrained strength are plotted against the anisotropy in correlation length $\alpha = L_H/L_V$ in Fig. 7. The lowest undrained strength is found for mixtures with correlation length anisotropy $L_H/L_V \approx 2$. A detailed analysis of numerical results shows that the trend in Fig. 7 reflects difficulties in shearing across 'vertical columns' when $L_H/L_V \ll 1$ or across 'horizontal layers' when $L_H/L_V \gg 1$. Note that the plane strain axial compression AC loading of a soil mass with anisotropy α corresponds to lateral compression LC loading of a soil mass with anisotropy $1/\alpha$ for the equivalent boundary conditions. Therefore the results in Fig. 7 provide insight into the effects of variability in LC loading.

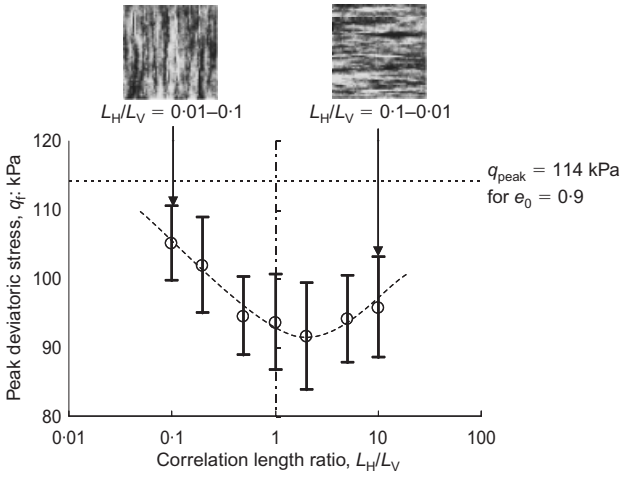

Fig. 7. Effect of anisotropy in correlation length on undrained shear strength. Longer correlation length kept constant at $L/D = 0{\cdot}1$. Mean trend and one-sigma ranges of numerical results are presented. Void ratio distribution is kept constant at $e_0 = 0{\cdot}8$–$1{\cdot}0$ (uniform distribution). Lighter colour indicates higher void ratio

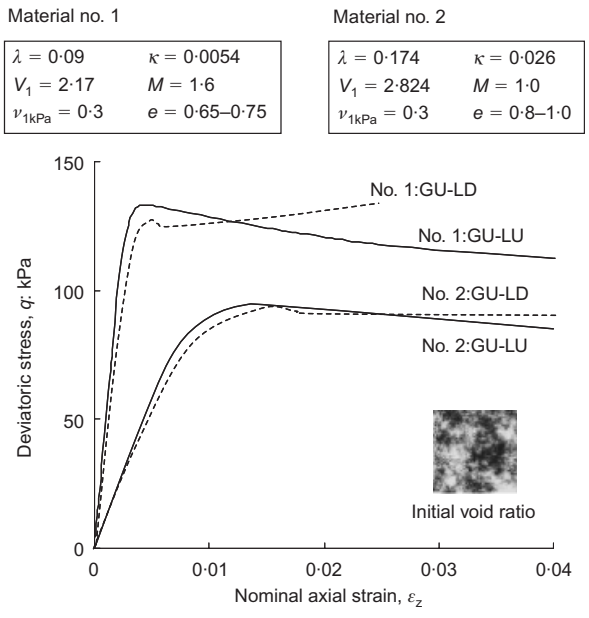

Fig. 6. Local drainage effects in correlated random media subjected to globally undrained deviatoric loading. GU (globally undrained), LD (locally drained) and LU (locally undrained). Initial void ratio is uniformly distributed. Correlation length $L/D = 0{\cdot}1$

Variation in initial void ratio distribution

The effect of the initial void ratio variability COV[e_0] is studied for realisations with the same correlation length ($L/D = 0{\cdot}16$) and the same mean void ratio $\mu[e_0] = 0{\cdot}9$ by varying the range in initial void ratio values. The mean values and two-sigma ranges in undrained shear strength obtained from 20 realisations for each COV[e_0] are shown in Fig. 8. The mean undrained shear strength decreases with

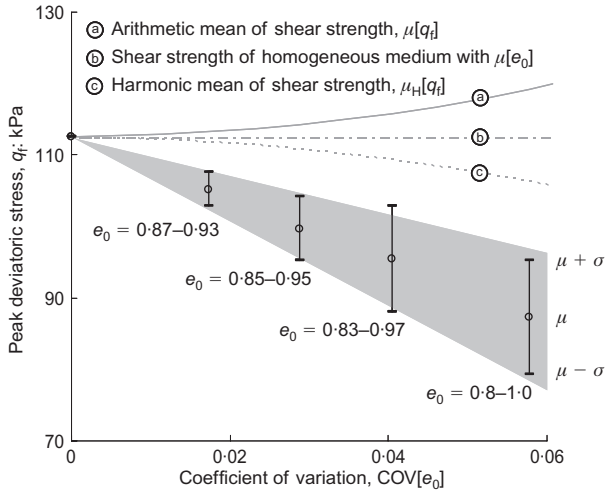

Fig. 8. Effects of COV in initial void ratio on undrained shear strength. Mean trend and one-sigma ranges of numerical results are presented. Analytical mixture model predictions are shown for comparison (lines a, b and c). Relative correlation length kept constant at $L/D = 0{\cdot}16$

the increase in COV[e_0] for a constant relative correlation length L/D. Griffiths *et al.* (2002) and Fenton & Griffiths (2003) report similar results with correlated random c–ϕ soil models.

While the harmonic mean of the local shear strength values is a good predictor of the global strength in uncorrelated binary mixtures (Fig. 2), the harmonic mean significantly overestimates the strength in correlated fields where interconnected weak zones facilitate shear localisation.

The assumed distribution affects the resultant undrained shear strength as well. For example, a Gaussian distribution of e_0 promotes higher mean undrained shear strength than the uniform distribution of e_0 with the same mean, variance and correlation length (Kim, 2005).

Correlation length effects L/D

The role of correlation length in the undrained shear strength is explored by varying the relative correlation length between $L/D = 0{\cdot}16$ and ~ 0, while keeping $\mu[e_0] = 0{\cdot}9$ and COV[e_0] $= 0{\cdot}06$ constant for a uniform e_0 distribution in the range $e_0 = 0{\cdot}9$ to $1{\cdot}0$. Fig. 9 shows the mean value and one-sigma ranges for the undrained shear strength against the relative correlation length L/D. The trend shows that longer correlation lengths lead to weaker media and higher variance among different realisations in the ensemble (see also Griffiths *et al.*, 2006). When the correlation length is infinitely longer than the specimen size $L/D \gg 1$, each realisation is a homogeneous medium, and the ensemble mean of the undrained shear strength for all realisations is the arithmetic mean of the initial q_{peak} distribution: in this case, $\mu[q_{peak}] = 114$ kPa for $L/D \rightarrow \infty$.

DRAINED RESPONSE

The study of the stress–strain response of correlated random media subjected to drained deviatoric loading follows a similar methodology: numerical runs in ABAQUS using the Modified Cam-Clay model (parameters in Table 1), and multiple realisations of correlated random fields in terms of the initial void ratio e_0.

Contractive media: strain-driven homogenisation

Multiple realisations of two-dimensional correlated scalar random fields are generated for an initial void ratio that follows a uniform distribution with a mean value $\mu[e_0] = 0{\cdot}9$, coefficient of variation COV[e_0] $= 0{\cdot}06$, and relative correlation length $L/D = 0{\cdot}10$. The lateral confinement throughout the test is equal to the initial isotropic confinement $\sigma'_0 = 100$ kPa; the corresponding critical-state void ratio is $e_{cs} = 0{\cdot}77$.

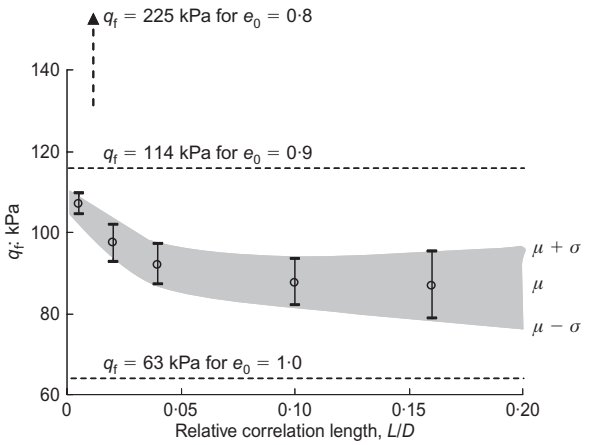

Fig. 9. Effect of correlation length on undrained shear strength. Specimens consolidated to $\sigma'_0 = 100$ kPa. Mean trend and one-sigma ranges of numerical results are presented. Uniform void ratio distribution $e_0 = 0{\cdot}8$–$1{\cdot}0$

Figure 10 presents the stress–strain curve and the shear strain field at various deformation levels for one realisation of a correlated random field. The weaker zones deform first and experience volumetric contraction, leading to an increase in shear strength, eventually approaching the load deformation of the homogeneous specimen with mean void ratio at intermediate strain levels. This local strain-hardening reduces the spatial contrast in strength distribution and hinders shear strain localisation. Gradually, the whole medium becomes homogenised, and the strength evolves towards the plane-strain critical-state strength of the homogeneous medium with $e_0 = 0{\cdot}9$. The b-value, where $b = (\sigma'_2 - \sigma'_3)/(\sigma'_1 - \sigma'_3)$, increases from $b \approx 0{\cdot}29$ at $\varepsilon_z = 0{\cdot}01$ to $b \approx 0{\cdot}45$ at $\varepsilon_z = 0{\cdot}1$.

The evolution in local void ratio during drained shear confirms strain-driven homogenisation. Fig. 11 displays the results for one realisation. The cumulative void ratio distributions at selected strain levels in Fig. 11 reveal the preferential contraction of looser elements first, and the evolution of homogenisation towards the critical-state void ratio. Fig. 12 confirms the evolution towards the critical state in p'–q–e space for the realisation shown in Fig. 10. For comparison, the p'–q–e path for the homogeneous specimen with $e_0 = 0{\cdot}9$ is shown as well.

The influence of the mean $\mu[e_0]$, the coefficient of variation COV[e_0], and the relative correlation length L/D on the drained shear response is explored in Fig. 13. Cases b, c and e are the stress–strain responses for three different mean initial void ratios $\mu[e_0]$, with the same initial variability and correlation length $L/D = 0{\cdot}10$. The trends for corresponding homogeneous cases with the same mean initial void ratios are shown beyond $\varepsilon_z = 0{\cdot}06$ in the figure. The stress–strain curves of the heterogeneous cases converge to those of homogeneous cases when the global axial strain exceeds $\varepsilon_z \approx 0{\cdot}05$ for the examples shown in Fig. 13.

Cases c and d show the influence of COV[e_0]. Higher strain is required to attain internal homogenisation in specimen with higher initial variability. Finally, realisations a and b show the effect of relative correlation length L/D in the specimen with the same initial mean void ratio and variability. It can be seen that specimens with longer correlation length require larger strains to attain internal homogenisation.

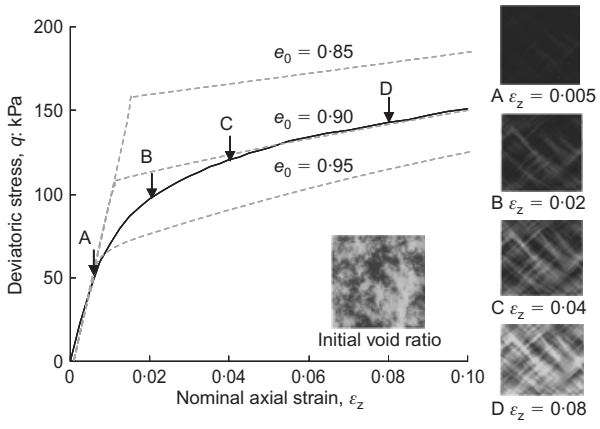

Fig. 10. Internal strain evolution in heterogeneous media subjected to drained deviatoric loading under $\sigma'_3 = 100$ kPa. Uniform initial void ratio range $e_0 = 0{\cdot}8$ to $1{\cdot}0$; $L/D = 0{\cdot}1$. Lighter colour indicates higher shear strain and higher void ratio. Dotted lines are for homogeneous media at the indicated void ratios. Note: $e_{cs} = 0{\cdot}77$; strain level shown to 10% only

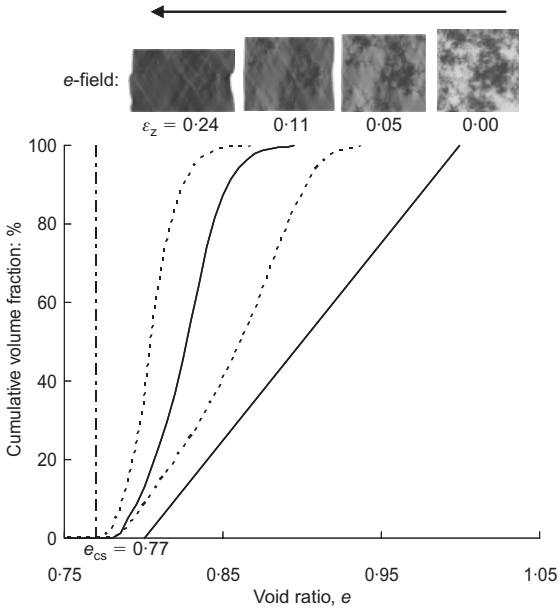

Fig. 11. Void ratio fields and cumulative distributions during drained deviatoric loading under $\sigma_3' = 100$ kPa for realisation with $L/D = 0{\cdot}1$ and uniform initial void ratio distribution between $e_0 = 0{\cdot}8$ and 1·0. Lighter colour indicates higher void ratio (black: 0·75, white: 1·00). The inclined straight line for the initial condition at $\varepsilon_2 = 0$ corresponds to the assumed uniform distribution

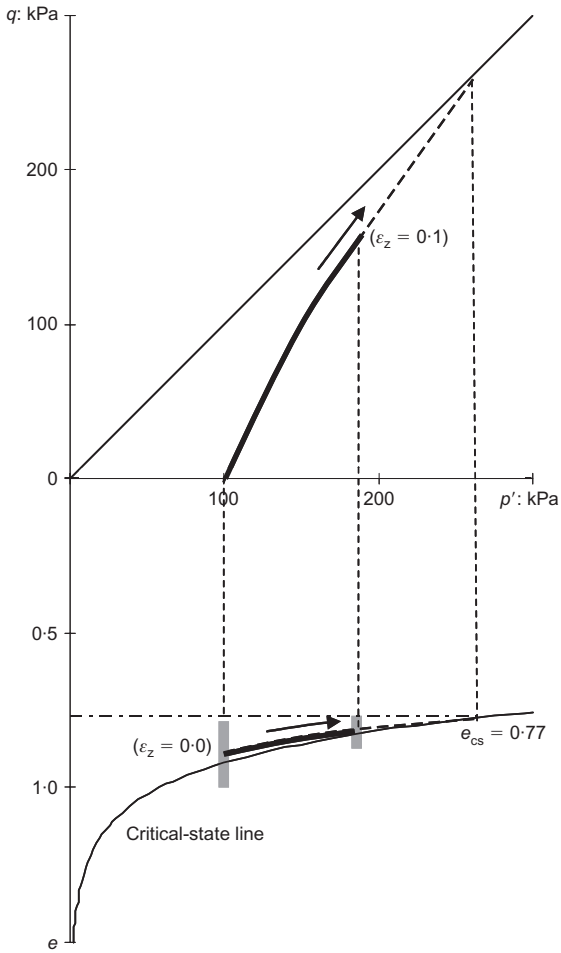

Fig. 12. Evolution of void ratio in p'–q–e space for contractive heterogeneous specimen subjected to drained deviatoric loading. Dotted lines show homogeneous specimen response (void ratio 0·90).

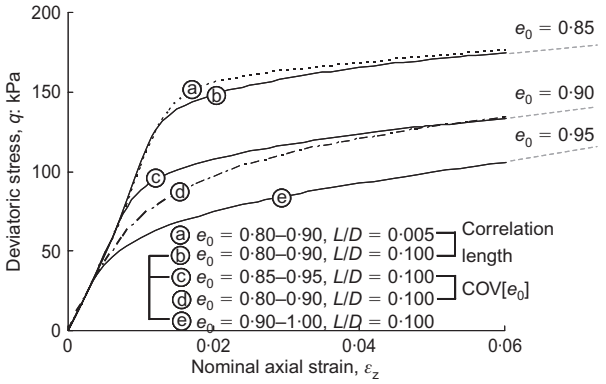

Fig. 13. Stress–strain response of contractive heterogeneous media subjected to plane-strain drained deviatoric loading under $\sigma_3' = 100$ kPa. Light-grey dotted lines shown beyond $\varepsilon_z = 0{\cdot}06$ are for homogeneous media at indicated initial void ratios. Note: $e_{cs} = 0{\cdot}77$; strain level shown to 6% only

Dilative media

The previous study is repeated for dilative media subjected to drained, plane-strain deviatoric loading. The critical-state void ratio for this stress path is $e_{cs} = 0{\cdot}77$: therefore the initial void ratio distribution $e_0 = 0{\cdot}7$ to 0·8 corresponds to a specimen with 70% of its volume on the dilative side. The stress–strain curve is shown in Fig. 14. The shear strain concentrates along interconnected internal weakness, as can be inferred by comparing initial void ratio fields and the corresponding shear strain fields (see Fig. 14). Clear shear strain localisation begins to manifest itself just before the peak of the stress–strain curve when a minimum b-value is reached: $b = 0{\cdot}27$. Cumulative void ratio distributions gathered at various strain levels are compared in Fig. 15. Drained shear loading causes volume contraction inside the yield surface, even for dense elements. Thereafter the void ratio increases in a few elements within the shear zone as the medium is loaded to failure. The p'–q–e paths for individual elements (not shown here) exhibit pronounced differences when the deviatoric load approaches and exceeds the peak values. Some elements in the shear zone experience a significant decrease in the effective mean stress, and reach critical state at low p' and high e_{cs} values. The global p'–q–e path for the specimen in Figs 14 and 15 is plotted in

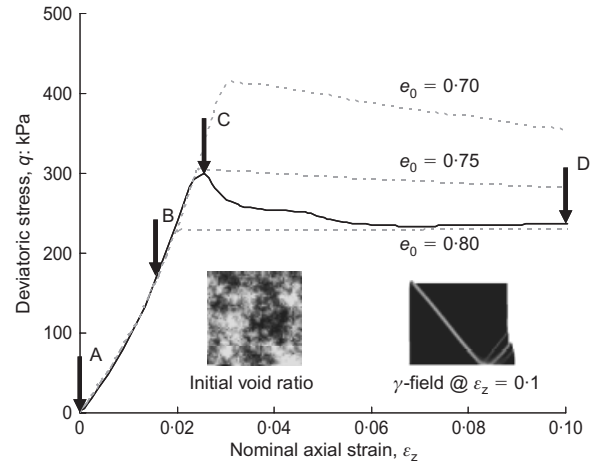

Fig. 14. Stress–strain response of dilative heterogeneous medium subjected to drained deviatoric plane-strain loading under $\sigma_3' = 100$ kPa. Uniform initial void ratio ranges $e_0 = 0{\cdot}7$–$0{\cdot}8$; $L/D = 0{\cdot}1$. Lighter areas indicate higher void ratio or shear strain. Dotted lines are for homogeneous media with various initial void ratios

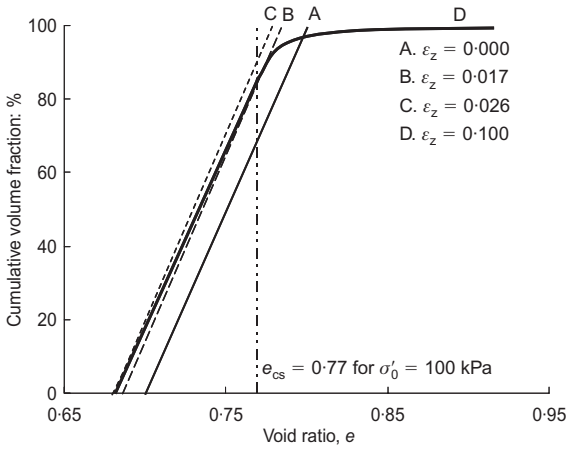

Fig. 15. Local void ratio distribution of dilative heterogeneous medium subjected to drained shear loading. Distributions A, B, C and D correspond to states shown in Fig. 14

Fig. 16. For comparison, the p'–q–e path for the homogeneous specimen with $e_0 = 0{\cdot}75$ is included in the figure. Clearly, strain localisation prevents the specimen from reaching the global critical-state void ratio (see experimental results in Desrues *et al.*, 1996).

SUMMARY AND CONCLUSIONS

Spatial variability in strength-determining soil parameters exerts different effects on the drained and undrained load–deformation responses. In this study, the initial void ratio is selected as a random variable to capture the spatial variability in strength. The following conclusions can be drawn from the numerical results.

(*a*) The mean global undrained shear strength decreases with increasing variance in the initial void ratio distribution. Spatial correlation causes a further decrease in undrained strength as compared with uncorrelated specimens with the same mean and variance.
(*b*) Shear strain localisation is triggered along neighbouring weak zones during undrained deviatoric loading. As the correlation length increases, the number of strong elements inside the shear zone decreases, and more pronounced shear bands develop.
(*c*) Anisotropy in the correlation length promotes undrained shear strength anisotropy.
(*d*) Drained deviatoric loading prompts the local deformation of weaker zones first. This phenomenon leads to internal homogenisation during drained shear when the whole medium is primarily contractive. The strain required to attain internal homogenisation increases as the variability or correlation length increase.
(*e*) When a spatially varying dilative medium is subjected to drained deviatoric loading, the shear strain concentrates along neighbouring weak zones and hinders homogenisation.
(*f*) Spatial variability implies an internal length scale that may allow for local drainage even when the overall conditions impose globally undrained shear. Looser elements gain strength at the expense of strength reduction in denser elements. These internal mechanisms affect the load–deformation response and strain localisation.
(*g*) The interpretation of measured boundary values in both experimental and numerical studies requires careful scrutiny in the context of spatially varying media.

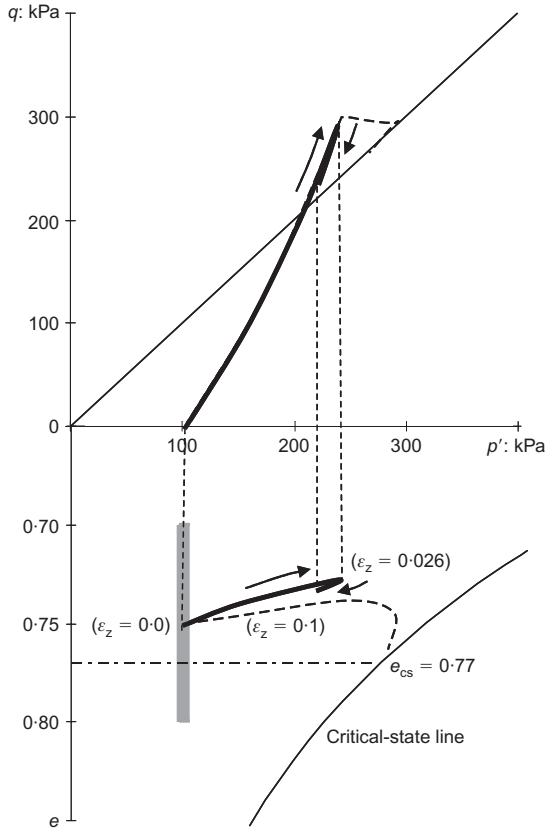

Fig. 16. Evolution of void ratio in p'–q–e space for dilative heterogeneous specimen subjected to drained deviatoric loading. Dotted lines show homogeneous specimen response (void ratio 0·75)

ACKNOWLEDGEMENTS

This research was supported by a grant on Scale Effects in Soils from the National Science Foundation. Additional support was provided by the Goizueta Foundation. Anonymous reviewers provided insightful comments and suggestions.

NOTATION

A	covariance matrix
C	Choleski decomposition matrix
COV	coefficient of variation
D	specimen size
d_{ij}	distance between points i and j
e_0	void ratio (e_0 initial, e_{cs} at critical state)
$F_R(\cdot)$	marginal probability distribution function
$F_x(\cdot)$	Gaussian probability distribution function
G	elastic shear modulus
L	correlation length
$\underline{l}$	location vector
L/D	relative correlation length
M	stress ratio at critical state
p'	mean effective stress
q	deviatoric stress ($q_{@all}$ average for the whole specimen; $q_{@b}$ computed in terms of boundary values; q_{peak}, peak deviatoric stress; q_f shear strength)
R	random number from 0-to-1
$R(\cdot)$	non-Gaussian scalar random field
$T(\cdot)$	trend
V_l	specific volume
V_{weak}	volume fraction of the weak material
$X(\cdot)$	Gaussian scalar random field
ε_z	nominal axial strain
$\varepsilon(\cdot)$	uncorrelated Gaussian random field of zero mean and unit variance

$\bar{\sigma}'$ length-averaged normal effective stress applied at boundaries
κ slope of swelling-recompression line
λ slope normal consolidation and critical state lines
ν Poisson's ratio (ν_{1kPa} Poisson's ratio at 1kPa effective confining)
σ standard deviation
$\mu[\cdot]$ arithmetic mean
$\mu_H[\cdot]$ harmonic mean

REFERENCES

Alshibli, K. A., Batiste, S. N. & Sture, S. (2003). Strain localization in sand: plane strain versus triaxial compression. *J. Geotech. Geoenviron. Engng ASCE* **129**, No. 6, 483–494.

Andrade, J. E. & Borja, R. I. (2006). Capturing strain localization in dense sands with random density. *Int. J. Numer. Methods Engng* **67**, No. 11, 1531–1564.

Ang, A. H. S. & Tang, W. H. (1975). *Probability concept in engineering planning and design*, Vol. 1, pp. 170–218. New York: John Wiley.

Antonellini, M. A., Aydin, A. & Pollard, D. D. (1994a). Microstructure of deformation bands in porous sandstones at Arches National Park, Utah. *J. Struct. Geol.* **16**, No. 7, 941–959.

Antonellini, M. A., Aydin, A., Pollard, D. D. & D'Onfro, P. (1994b). Petrophysical study of faults in sandstones using petrographic image analysis and X-ray computerized tomography. *Pure Appl. Geophys.* **143**, Nos 1–3, 181–201.

Bhatia, K. S. & Soliman, A. F. (1990). Frequency distribution of void ratio of granular materials determined by an image analyzer. *Soils Found.* **30**, No. 1, 1–16.

Cho, G. C., Lee, J. S. & Santamarina, J. C. (2004). Spatial variability in soils: high resolution assessment with electrical needle probe. *J. Geotech. Geoenviron. Engng ASCE* **130**, No. 8, 843–850.

DeGroot, D. J. (1996). Analyzing spatial variability of in-situ soil properties. In *Uncertainty in the geologic environment* (eds C. D. Shackelford, P. P. Nelson and M. J. S. Roth), pp. 210–238. Geotechnical Special Publication No. 58, ASCE.

DeGroot, D. J. & Baecher, G. B. (1993). Estimating autocovariance of in-situ soil properties. *J. Geotech. Engng Div. ASCE* **119**, No. 1, 147–166.

Desrues, J. (1998). Localization patterns in ductile and brittle geomaterials. In *Material instabilities in solids* (eds R. Borst and E. Geissen), pp. 137–158. Malden, MA: Wiley-Interscience.

Desrues, J., Chambon, R., Mokni, M. & Mazerolle, F. (1996). Void ratio evolution inside shear bands in triaxial sand specimens studied by computed tomography. *Géotechnique* **46**, No. 3, 529–546.

El-Kadi, A. I. & Williams, S. A. (2000). Generating two-dimensional fields of auto-correlated, normally distributed parameters by the matrix decomposition technique. *Ground Water* **38**, No. 4, 530–532.

Fenton, G. A. (1994). Error evaluation of three random field generators. *ASCE J. Engng Mech.* **120,** No. 12, 2487–2497.

Fenton, G. A. & Griffiths, D. V. (2003). Bearing capacity prediction of c–ϕ soils. *Can. Geotech. J.* **41**, No. 2, 368–369.

Finno, R. J., Harris, W. W., Mooney, M. A. & Viggiani, G. (1997). Shear band in plane strain compression of loose sand. *Géotechnique* **47**, No. 1, 149–165.

Griffiths, D. V., Fenton, G. A. & Tveten, D. E. (2002). Probabilistic geotechnical analysis: How difficult does it need to be? Keynote paper. *Proceedings of UEF conference on probabilistics in geotechnics: Technical and economic risk estimation*, Graz.

Griffiths, D. V., Fenton, G. A. & Zeimann, H. R. (2006). Seeking out failure: the random finite element method (RFEM) in probabilistic geotechnical analysis. *Proc. ASCE GeoCongress 2006 Conf.*, Atlanta, GA.

Grigoriu, M. (1984). Crossing of non-Gaussian translation process. *ASCE J. Engng Mech.* **110**, No. 4, 610–620.

HKS (2006). *ABAQUS/Standard: User's Manual, Ver. 6·6*. Rhode Island: Habbit, Karlsson & Sorenson, Inc..

Han, C. & Valdoulakis, I. (1991). Plane-strain compression experiments on water-saturated fine-grained sand. *Géotechnique* **41**, No. 1, 49–78.

Harr, M. E. (1987). *Reliability-based design in civil engineering*. New York: McGraw-Hill.

Hegazy, A. H., Mayne, P. M. & Rouhani, S. (1996). Geostatistical assessment of spatial variability in piezocone tests. In *Uncertainty in the geologic environment* (eds C. D. Shackelford, P. P. Nelson and M. J. S. Roth), pp. 254–268. Geotechnical Special Publication No. 58, ASCE.

Hicks, M. A. & Onisiphorou, C. (2005). Stochastic evaluation of static liquefaction in a predominantly dilative sand fill. *Géotechnique* **55**, No. 2, 123–133.

Hicks, M. A. & Samy, K. (2002). Influence of heterogeneity on undrained clay slope stability. *Q. J. Engng. Geol. Hydrogeol*. **35**, No. 1, 41–49.

Hoeg, K., Dyvik, R. & Sandbaekken, G. (2000). Strength of undisturbed versus reconstituted silt and silty sand specimens. *J. Geotech. Geoenviron. Engng ASCE* **126**, No. 7, 606–617.

Ishihara, K. (1993). Liquefaction and flow failure during earthquakes. *Géotechnique* **43**, No. 3, 351–415.

Jang, D. J. (1997). *Quantification of sand structure and its evolution during shearing using image analysis.* PhD dissertation, School of Civil and Environmental Engineering, Georgia Institute of Technology, Atlanta.

Jang, D. J., Frost, J. D. & Park J. Y. (1999). Preparation of epoxy impregnated sand coupons for image analysis. *Geotech. Test. J. ASTM* **22**, No. 2, 147–158.

Jones, A. L., Kramer, S. L. & Arduino, P. (2002). *Estimation of uncertainty in geotechnical properties for performance-based earthquake engineering*. PEER report 2002/16. University of California, Berkeley: Pacific Earthquake Engineering Research Center.

Kim, H.-K. (2005). *Spatial variability in soils: Stiffness and strength*. PhD dissertation. School of Civil and Environmental Engineering, Georgia Institute of Technology, Atlanta.

Kulhawy, F. H. (1992). On evaluation of static soil properties. In *Stability and performance of slopes and embankments II* (eds R. B. Seed and R. W. Boulanger), Geotechnical Special Publication No. 31, ASCE, pp. 95–115.

Lacasse, S. & Nadim, F. (1996). Uncertainties in characterizing soil properties. In *Uncertainty in the geologic environment* (eds C. D. Shackelford, P. P. Nelson and M. J. S. Roth), pp. 49–75. Geotechnical Special Publication No. 58, ASCE.

Ladd, R. S. (1974). Specimen preparation and cyclic stability of sands. *J. Geotech. Engng Div. ASCE* **100**, No. 10, 1180–1184.

Lade, P. V. & Wang, Q. (2001). Analysis of shear banding in true triaxial tests on sand. *J. Engng Mech. ASCE* **127**, No. 8, 762–768.

Mulilis, J. P., Chan, C. K. & Seed, H. B. (1975). *The effects of method of sample preparation on the cyclic stress–strain behavior of sands*, EERC Report No. 75-18. University of California, Berkeley: College of Engineering.

Nübel, K. & Karcher, C. (1998). FE simulations of granular material with a given frequency distribution of voids as initial condition. *Granular Matter* **1**, No. 3, 105–122.

Phoon, K. K. & Kulhawy, F. H. (1999). Characterization of geotechnical variability. *Can. Geotech. J.* **36**, No. 4, 612–624.

Popescu, R., Prevost, J. H. & Deodatis, G. (1997). Effects of spatial variability on soil liquefaction: some design recommendations. *Géotechnique* **47**, No. 5, 1019–1036.

Popescu, R., Prevost, J. H. & Deodatis, G. (2005). 3D effects in seismic liquefaction of stochastically variable soil deposits. *Géotechnique* **55**, No. 1, 21–31.

Ravi, V. (1992). Statistical modeling of spatial variability of undrained strength. *Can. Geotech. J.* **29**, No. 5, 721–729.

Rechenmacher, A. L. (2006). Grain-scale processes governing shear band initiation and evolution in sands. *J. Mech. Phys. Solids* **54**, No. 1, 22–45.

Rechenmacher, A. L. & Medina-Cetina, Z. (2007). Calibration of soil constitutive models with spatially varying parameters. *J. Geotech. Geoenviron. Engng ASCE* **133**, No. 12, 1567–1576.

Rechenmacher, A. L., Medina-Cetina, Z. & Ghanem, R. G. (2005). Calibration of heterogeneous, probabilistic soil models. *Proc. 16th Int. Conf. Soil Mech. Geotech. Engng, Osaka* **2**, 851–854.

Roscoe, K. H. & Burland, J. B. (1968). On the generalized stress–strain behaviour of wet clay. In *Engineering plasticity* (eds

J. Heyman and F. A. Leckie), pp. 535–609. London: Cambridge University Press.

Shahinpoor, M. (1981). Statistical mechanical considerations on storing bulk solids. *Bulk Solids Handling* **1**, No. 1, 31–36.

Tang, W. (1979). Probabilistic evaluation of penetration resistance. *J. Geotech. Engng ASCE* **105**, No. GT10, 1173–1191.

Townsend, F. C. (1978). A review of factors affecting cyclic triaxial tests. In *Dynamic geotechnical testing*, pp. 356–383. Special Technical Publication, No. 654, ASTM.

Vaid, Y. P. & Sivathayalan, S. (2000). Fundamental factors affecting liquefaction susceptibility of sands. *Can. Geotech. J.* **37**, No. 3, 592–606.

Vaid, Y. P., Uthayakumar, M., Sivathayalan, S., Robertson, P. K. & Hofmann, B. (1995). Laboratory testing of Syncrude sand. *Proc. 48th Can. Geotech. Conf., Vancouver* **1**, 223–232.

Vanmarcke, E. H. (1977). Probabilistic modeling of soil profiles. *J. Soil Mech. Found. Div. ASCE* **103**, No. GT11, 1227–1246.

Vardoulakis, I., Goldscheider, M. & Gudehus, G. (1978). Formation of shear bands in sand bodies as a bifurcation problem. *Int. J. Numer. Anal. Methods Geomech.* **2**, No. 2, 99–128.

Vio, R., Andreani, P. & Wamsteker, W. (2001). Numerical simulation of non-Gaussian random fields with prescribed correlation structure. *Pub. Astronom. Soc. Pacific* **113**, 1009–1020.

Yamazaki, F. & Shinozuka, M. (1988). Digital generation of non-Gaussian stochastic fields. *ASCE J. Engng Mech.* **114**, No. 7, 1183–1197.

Yang, X. (2005). *Three-dimensional characterization of inherent and induced sand microstructure.* PhD dissertation, School of Civil and Environmental Engineering, Georgia Institute of Technology, Atlanta.

Yoshida, T., Tatsuoka, F., Siddiquee, M. S. A., Kamegai, Y. & Park, C.-S. (1993). Shear banding in sands observed in plane strain compression. *Proc. 3rd Int. Workshop on Localization and Bifurcation Theory for Soils and Rocks, Grenoble*, 165–179.

Zaoui, A. (2002). Continuum micromechanics: survey. *J. Engng Mech. ASCE* **128**, No. 8, 808–816.